Data on $\bar{p}p \to \eta'\pi^0\pi^0$ for masses 1960 to 2410 MeV

A.V. Anisovich [c] C.A. Baker [b] C.J.Batty [b] D.V. Bugg [a], C.Hodd [b] V.A. Nikonov [c], A.V. Sarantsev [c], V.V. Sarantsev [c], B.S. Zou [a,1]

[a] *Queen Mary and Westfield College, London E1 4NS, UK*

[b] *Rutherford Appleton Laboratory, Chilton, Didcot, OX11 OQX, UK*

[c] *St. Petersburg Nuclear Physics Institute, Gatchina, St. Peterburg district, Russia 188350*

Abstract

Data on $\bar{p}p \to \eta'(958)\pi^0\pi^0$ are presented at nine $\bar{p}$ momenta from 600 to 1940 MeV/c. Strong S-wave production of $f_2(1270)\eta'$ is observed, requiring a $J^{PC} = 2^{-+}$ resonance with mass $M = 2248 \pm 20$ MeV, $\Gamma = 280 \pm 20$ MeV.

[1] Now at the Institute for High Energy Physics, Beijing 100039, China

The first data are presented on $\bar{p}p \to \eta'\pi^0\pi^0$ in flight. These data were taken with the Crystal Barrel detector at LEAR. They are part of an extensive study of the $I = 0$, $C = +1$ system in several channels. Data have been reported earlier on $\pi^0\pi^0$ [1], $\eta\eta$ and $\eta\eta'$ [2], and $\eta\pi^0\pi^0$ [3]. A comparison will be made here specifically with the $\eta\pi^0\pi^0$ data, and with a combined amplitude analysis of all the earlier data [4].

The experimental set-up has been reported in detail [5]. A $\bar{p}$ beam from LEAR interacts in a liquid hydrogen target 4.4 cm long at the centre of the detector. Incident $\bar{p}$ are counted by a coincidence between a scintillator of 5 mm diameter and a small multiwire proportional chamber, both positioned $\sim$ 5 cm upstream of the target. Two veto counters 20 cm downstream of the target provide a trigger for interactions. The target is surrounded over 98% of the solid angle by a multiwire proportional chamber and a silicon vertex detector. These provide an on-line trigger for neutral final states. With a $\bar{p}$ beam of $\sim 2 \times 10^5$/s, the trigger rate is $\sim$ 60/s.

The present channel is studied in 10γ events, where $\eta' \to \eta\pi^0\pi^0$, $\eta \to \gamma\gamma$. Photons are detected with high efficiency down to 20 MeV in a barrel of 1380 CsI crystals covering 98% of the solid angle; the geometry is such that crystals point towards the target. The crystals have a length of 16 radiation lengths and provide an angular resolution of ± 20 mrad in azimuth and polar angle. The energy resolution is given by $\Delta E/E = 2.5\%/E(\mathrm{GeV})^{1/4}$.

The general procedures for event reconstruction and selection have been described in several earlier publications, of which the most detailed concern the study of $\pi^0\pi^0$, $\eta\eta$ and $\eta\eta'$ final states [1,2]. A Monte Carlo simulation of the detector is used to assess the efficiency for reconstruction of the $\pi^0\pi^0\eta'$ final state and the levels of background from competing channels.

Events are first submitted to a kinematic fit to $\bar{p}p \to 10\gamma$, requiring a confidence level $> 5\%$. Next a kinematic fit to $\bar{p}p \to \eta 4\pi^0$ is required, again with confidence level $> 5\%$. At this stage, the main background comes from $5\pi^0$ events. This background is suppressed strongly by rejecting any event passing a kinematic fit to $5\pi^0$ with confidence level $> 1\%$ (or 0.1% at 600 MeV/c, where the background is more severe). Finally, those few events are rejected which fit $\eta\eta 3\pi^0$ with confidence level better than $\eta 4\pi^0$.

Fig. 1 shows the $\eta\pi\pi$ mass distribution of surviving events in the mass range around the η'. There is a clear η' signal, agreeing in mass within ≤ 4 MeV with the standard value at all momenta. It is superposed on a smooth background, whose magnitude is largest at low momenta. The Monte Carlo simulation estimates that the background comes approximately equally from 3 sources: (i) $5\pi^0$ events, (ii) $\omega 4\pi^0$, ($\omega \to \pi^0\gamma$) after losing one photon, and (iii) $\eta 5\pi^0$ after losing two photons. The predicted background agrees well with that observed, within 10% of its magnitude. Tighter cuts do not improve the signal/background ratio significantly, but simply cause loss of events.

Signal events are selected from the peak region of the η' by adjusting a mass cut around the peak at every individual momentum so as to optimise the signal/background ratio. Statistics of the data selection are shown in Table 1. In the maximum likelihood fit used for amplitude analysis, sidebins events shown shaded in Fig. 1 are used to subtract the background. The areas of sidebins are chosen so that each covers twice the range of mass squared which is used to select η' events. A technicality arises in the data processing. Reconstructed π^0 are sorted according to the accuracy with which their energy is determined. The width of the mass cut is varied according to the accuracy with which the η' mass is reconstructed. This is the reason that sidebands have diffuse edges. Technically, the way the subtraction is made is to include sidebin events into the fit with a weight -0.25 times that of events selected in the signal region. Amplitudes are constructed with tensor expressions using the measured mass of each η'.

Momentum (MeV/c)	Data	BG	Signal	ϵ (%)
600	207	77	130	2.90
900	1017	399	618	4.61
1050	785	260	525	5.76
1200	2770	852	1918	6.33
1350	2296	595	1701	5.92
1525	1429	312	1117	5.06
1642	1530	330	1200	4.72
1800	1503	325	1178	4.57
1940	1083	263	820	4.34

Table 1
Numbers of selected events, estimated background (BG), true signal, and reconstrucion efficiency ϵ as a function of beam momentum.

Fig. 2 shows the Dalitz plots at all momenta for events from the signal region. There is an obvious contribution due to $f_2(1270)\eta'$, appearing at momenta of 1200 MeV/c upwards. Fig. 3 shows the Dalitz plots for sidebin events. The distribution of background is not uniform, but peaks in the corners of the Dalitz plots. This peaking accounts for corresponding peaks observed in the corners of the Dalitz plots of Fig. 2. When the subtraction is made, the surviving signal outside the $f_2(1270)$ peak is nearly uniform within the available statistics. There is no indication for the presence of $a_2(1320) \rightarrow \eta'\pi$. The expected contribution may be predicted from fits with have been made to $a_2(1320)\pi$ in $\eta\pi^0\pi^0$ data [3]. The predicted contribution is only $\sim 3\%$ of $\eta'\pi^0\pi^0$, because of the small (0.53%) branching fraction of $a_2(1320)$ to $\eta'\pi$. This contribution is included in the amplitude analysis using amplitudes fitted to the $\eta\pi\pi$ data, but is so small as to have negligible effect on conclusions. Fig. 4 shows projections at two beam momenta on to masses of $\pi\pi$ and $\pi\eta$; the latter is featureless. The histograms show results of the maximum likelihood fit described below.

Points on Fig. 5 shows the integrated $\eta'\pi^0\pi^0$ cross section after background subtraction and after correction for all unobserved decay modes of η', η and π^0. There is a peak around 2230 MeV, which is the nominal threshold for $f_2(1270)\eta'(958)$. The absolute normalisation is obtained using beam counts, target length and density, and correcting the observed number of signal events for the reconstruction efficiency shown in Table 1. A correction is applied for observed rate dependence of the cross section, as described in detail in Ref. [1].

The amplitude analysis is made using (a) S and P-waves for $\sigma\eta'$, where σ stands for the $\pi\pi$ S-wave amplitude, for which we use the parametrisation of Zou and Bugg [6], (b) S and P-waves for $f_2(1270)\eta'$, and (c) a small, almost negligible contribution from ${}^3P_1 \to f_0(975)\eta'$, which helps marginally in fitting the $\pi\pi$ mass distribution at the lowest three beam momenta. It is to be expected that higher partial waves for $f_2\eta'$ will be suppressed strongly by the centrifugal barrier in the final states. Contributions from D-waves have been tried in the fit, but are not required; indeed, the P-wave contribution is quite small. Likewise, $\sigma\eta'$ contributions with $L \geq 2$ are negligible.

We shall present amplitudes for $f_2(1270)\eta'$ in partial waves ${}^1D_2$ ($J^{PC} = 2^{-+}$), ${}^3P_2$ and ${}^3F_2$ (2^{++}), ${}^3P_1$ (1^{++}) and ${}^3F_3$ (3^{++}); they will be compared with $f_2(1270)\eta$ observed in $\eta\pi\pi$ data [3,4]. These two channels are related by the composition of the η' and η in terms of strange and non-strange quarks:

$$|\eta> \simeq 0.8\frac{u\bar{u} + d\bar{d}}{\sqrt{2}} - 0.6s\bar{s}, \tag{1}$$

$$|\eta'> \simeq 0.6\frac{u\bar{u} + d\bar{d}}{\sqrt{2}} + 0.8s\bar{s}. \tag{2}$$

The coefficients 0.8 and 0.6 are derived from the well known pseudo-scalar mixing angle [7]. Our earlier analysis of $\bar{p}p \to \pi^-\pi^+$, $\pi^0\pi^0$, $\eta\eta$ and $\eta\eta'$ [8] finds that almost all s-channel resonances produced in $\bar{p}p$ interactions are consistent with small mixing angles $\leq 15^\circ$ between $(u\bar{u} + d\bar{d})/\sqrt{2}$ and $s\bar{s}$. The naive prediction is therefore that amplitudes for $\bar{p}p \to f_2(1270)\eta'$ and $\bar{p}p \to f_2(1270)\eta$ will be related by

$$a(f_2\eta') \simeq 0.75a(f_2\eta). \tag{3}$$

The peak in Fig. 5(a) requires a resonance in $f_2\eta'$ close to the mass of the peak. However, the mass spectrum from a simple resonance will be pushed upwards by the rapidly increasing phase space for the final state $f_2\eta'$; this effect is visible in the dotted curve of Fig. 5(c), which peaks above 2300 MeV. In order to reproduce the integrated cross section of Fig. 5(a), the amplitude analysis requires a strong interfering background peaking below threshold. The interference is constructive at low masses, and is required to give a large $f_2\eta'$ cross section there, despite the limited phase space. Above the peak at 2230 MeV, the interference becomes destructive, and cuts off the $f_2\eta'$ cross section on the upper side of the resonance.

The motivation for this scenario arises from a new combined analysis [4] of $\eta\pi\pi$ data, together with those on $\bar{p}p \to \pi^-\pi^+$, $\pi^0\pi^0$, $\eta\eta$ and $\eta\eta'$. Results for $\eta\pi\pi$ from that analysis are shown in Fig. 5(b). This analysis requires a 2^{-+} resonance at 2251 ± 15 MeV. It appears there most clearly in $f_2(1270)\eta$ with $L = 2$ in the final state, shown by the chain curve in Fig.5(b). However, for the $f_2\eta$ S-wave channel, what one observes is a strong peak near 2 GeV, shown by the full curve. This comes mostly from $\eta_2(1860)$, but partly from $\eta_2(2030)$ reported in an analysis of data on $\bar{p}p \to \eta\pi^0\pi^0\pi^0$ [9]. The intensities of contributions to the $f_2\eta$ channel are shown in Fig. 5(b) from (i) $\eta_2(2260)$ (dotted curve) and (ii) the coherent sum of $\eta_2(1860)$ and $\eta_2(2030)$ (dashed curve); the latter two resonances are not well resolved by the $\eta\pi\pi$ data, because they lie close together near the $\bar{p}p$ threshold. The contribution from $\eta_2(2260)$ interferes destructively with $\eta_2(1860)$ and $\eta_2(2260)$, so as to cut off the full curve at high masses.

The width of the $\eta_2(2260)$ is well determined by the width of the peak in Fig. 5(a): $\Gamma = 280 \pm 20$ MeV. The mass is somewhat less well determined, since the interference with the tails of the lower resonances shifts the peak by an amount which is sensitive to their widths. Using the best estimates for the widths from Ref. [8], the mass of $\eta_2(2260)$ from the present data is $M = 2248 \pm 20$ MeV, in good agreement with the value derived from $\eta\pi\pi$ data. The Argand diagram for the $f_2\eta'$ S-wave amplitude is shown in Fig. 5(d).

A striking feature of the $f_2\eta'$ signal is its large magnitude. The dashed curve on Fig. 5(a) shows the complete integrated $\eta\pi^0\pi^0$ cross section, multiplied by $(0.75)^2$ to allow for the expected inhibition of η' with respect to η. It is surprising that the $f_2\eta'$ signal is nearly as strong as the dashed curve, bearing in mind the difference in available phase space for $f_2\eta'$ and $f_2\eta$. The peak in the $\eta'\pi\pi$ cross section (full curve) is much larger than the small peak observed at the same mass in the $\eta\pi\pi$ cross section. Likewise, the S-wave peak due to $\eta_2(2260) \to f_2\eta'$, shown by the dotted curve in Fig. 5(c), is considerably stronger than that in $f_2\eta$ in Fig. 5(b). If one takes into account the available phase space for $f_2\eta'$ and $f_2\eta$, the coupling constant for $\eta_2(2260) \to f_2\eta'$ relative to that in $f_2\eta$ is stronger than predicted by equn. (3) by a factor 5.2 for the amplitudes.

Vandermeulen has remarked that $\bar{p}p$ annihilation usually favours high mass final states [10]. This may be understood as a form factor effect, arising from the sizes of the participating states. In present data, the final state $f_2\eta'$ has very low momentum. However, in the process $\eta_2(2260) \to f_2\eta$, the momentum q in the final state is $\sim$ 635 MeV/c. The factor 5.2 would require a form factor $\exp -(4.1q^2)$ in amplitude, with q in GeV/c; if this arises from a source having a Gaussian distribution in r, the form factor takes the well known form $\exp -(q^2R^2/6)$, and requires a radius of interaction $R = 0.98$ fm. Such a form factor is surprisingly strong. For comparison, the Vandermeulen form factor approximates to $\exp -(1.5q^2)$.

The strong sub-threshold contribution to the $f_2\eta'$ S-wave is also intriguing. A variety of explanations are possible, of which we mention one. In Ref. [9], evidence has been presented for three η_2 resonances in a mass range where only two are likely to be $q\bar{q}$. Of these, $\eta_2(1860)$ is a candidate for a hybrid, because of its strong decay to $f_2\eta$, despite limited phase space. If that conjecture is correct, it should be accompanied by an $s\bar{s}g$ partner at about 2100 MeV. Such an $s\bar{s}g$ hybrid is expected to decay strongly to $f_2(1525)\eta'$ and $f_2(1270)\eta'$. If it mixes into neighbouring $q\bar{q}$ states, it could help to explain the anomalously strong $f_2\eta'$ signal observed here.

We now consider other partial waves. The present data require a small but significant P-wave $f_2\eta'$ contribution. This could arise from initial $\bar{p}p$ states ${}^3P_1$, ${}^3P_2$, ${}^3F_2$ or ${}^3F_3$. The amplitude analysis of Ref. [4] requires all of these contributions in $\eta\pi\pi$ data with a 2^+ resonance at 2300 MeV, a 1^+ resonance at $\sim$ 2275 MeV and 2^+ resonances at 2210 and 2285 MeV. A good fit to present data may be obtained by fixing the relative magnitudes and phases of these partial waves from the fit to $\eta\pi^0\pi^0$ data. The absolute magnitude of the P-wave contribution is sensitive to the radius chosen for the Blatt-Weisskopf centrifugal barrier. This radius is therefore adjusted to give the best fit to the data, with the reasonable result 0.8 fm.

The magnitudes of the contributions are then 3.5% for ${}^3F_3$, 3.2% for ${}^3P_1$, 3.2% for the 2^+ resonance at 2210 MeV and 1.0% for the 2^+ resonance at 2285 MeV; in the latter two, the ratios of amplitudes for ${}^3P_2$ and ${}^3F_2$ are taken from Ref. [4]. Without these amplitudes, log likelihood is worse by 142 for only one parameter fitted to the overall magnitude; so the P-wave contribution is highly significant. [Our definition of log likelihood is such that it a change of 0.5 corresponds to one standard deviation change in one variable]. If instead the magnitudes and phases of these amplitudes are fitted freely, the fit changes very little. It is not possible from the present data to separate ${}^3P_2$ and ${}^3F_2$, which need to be constrained in relative magnitude as determined in Ref. [4]. Then the freely fitted magnitudes are 3.9% for ${}^3F_3$, 4.7% for ${}^3P_1$ and 3.9%

for 2^+, close to the contrained fit. Log likelihood improves by 43, which is barely significant for 7 extra fitted parameters; changes in the fit to angular distributions are barely visible by eye.

Figs. 6(a) and (b) show angular distributions for production of $\eta' f_2(1270)$ in the mass range > 1.1 GeV in terms of the centre of mass angle θ of the η' The distributions are uncorrected for acceptance, which is included in the maximum likelihood fit shown by the histograms. At high beam momenta, the acceptance for η' falls in the forward direction, where the separation of its decay products becomes less efficient. A check on the reconstruction procedure is that angular distributions are symmetric forward-backward in the centre of mass system within errors, as required by charge conjugation invariance.

We now turn to the contributions from the broad $\sigma\eta'$ channel. From present data, the only firm conclusion which may be drawn is that contributions from both $^1S_0$ and $^3P_1$ initial states are required. At all momenta from 900 MeV/c upwards, the data require angular distributions of the form $A + B\cos^2\theta_{\eta'}$, as shown in Figs. 6(c) and (d). The $\eta\pi\pi$ data have been fitted including 0^- and 1^+ resonances. Present data are fitted well by the same resonances. However, statistics are not sufficient to provide clear evidence of these resonances in present data. Fig. 6 shows that the fit to data is adequate.

In summary, the main feature of the $\eta'\pi^0\pi^0$ data is a peak at 2230 MeV, requring a dominant contribution from the $f_2(1270)\eta'$ S-wave. The data require a 2^{-+} resonance with mass 2248 ± 20 MeV and width $\Gamma = 280 \pm 20$ MeV; this result is closely consistent with an $\eta_2(2260)$ resonance observed in $\eta\pi\pi$ data. The $f_2\eta'$ S-wave amplitude is surprisingly strong compared with that for $f_2\eta$, even allowing for a form factor in the latter. Contributions from $f_2(1270)\eta'$ P-states are consistent with the amplitude analysis of the $\eta\pi\pi$ data.

1 Acknowledgement

We thank the Crystal Barrel Collaboration for allowing use of the data. We wish to thank the technical staff of the LEAR machine group and of all participating institutes for their invaluable contribtuions to the successful running of the experiment. We acknowledge financial support from the British Particle Physics and Astronomy Research Council (PPARC). The St. Petersburg group wishes to acknowledge financial support from PPARC and INTAS grant RFBR 95-0267.

References

[1] A.V. Anisovich et al., Phys. Lett. B468 (1999) 304.

[2] A.V. Anisovich et al., Phys. Lett. B468 (1999) 309.

[3] A.V. Anisovich et al., Phys. Lett. B452 (1999) 180; Nucl. Phys. A651 (1999) 253.

[4] A.V. Anisovich et al., *Combined amplitude analysis of final states with $I = 0$, $C = +1$ in $\bar{p}p$ annihilation in flight*, submitted to Phys. Lett. B.

[5] E. Aker et al., Nucl. Instr. A321 (1992) 69.

[6] B.S. Zou and D.V. Bugg, Phys. Rev. D50 (1994) R3948.

[7] C. Amsler et al., Phys. Lett. B294 (1992) 451.

[8] A.V. Anisovich et al., Phys. Lett. B471 (1999) 271.

[9] A.V. Anisovich et al., *Three $I = 0$ $J^{PC} = 2^{-+}$ mesons*, Phys. Lett. B (in press).

[10] J. Vandermeulen, Z. Phys. C37 (1988) 563.

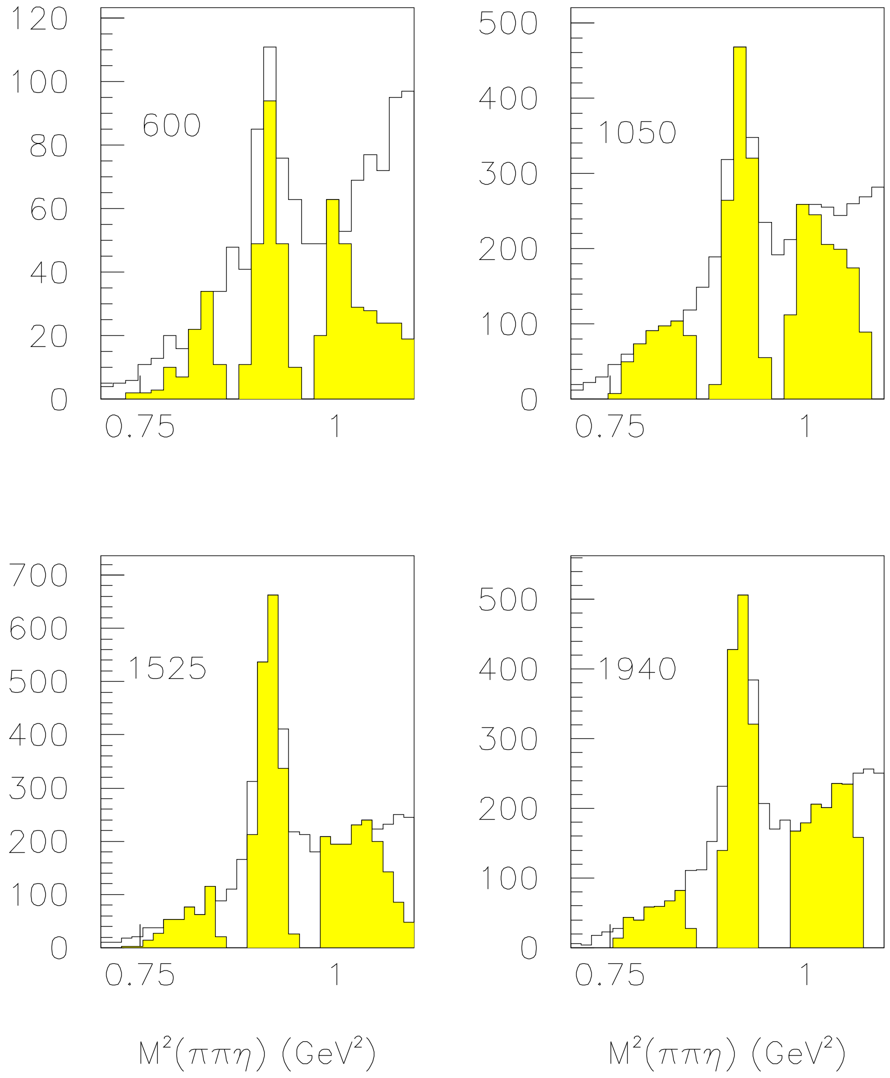

Fig. 1. The distribution of $M^2(\eta\pi\pi)$ at four beam momenta indicated by numerical values in MeV/c. The shaded areas show selected signal events in the η' peak and those used for sideband subtraction.

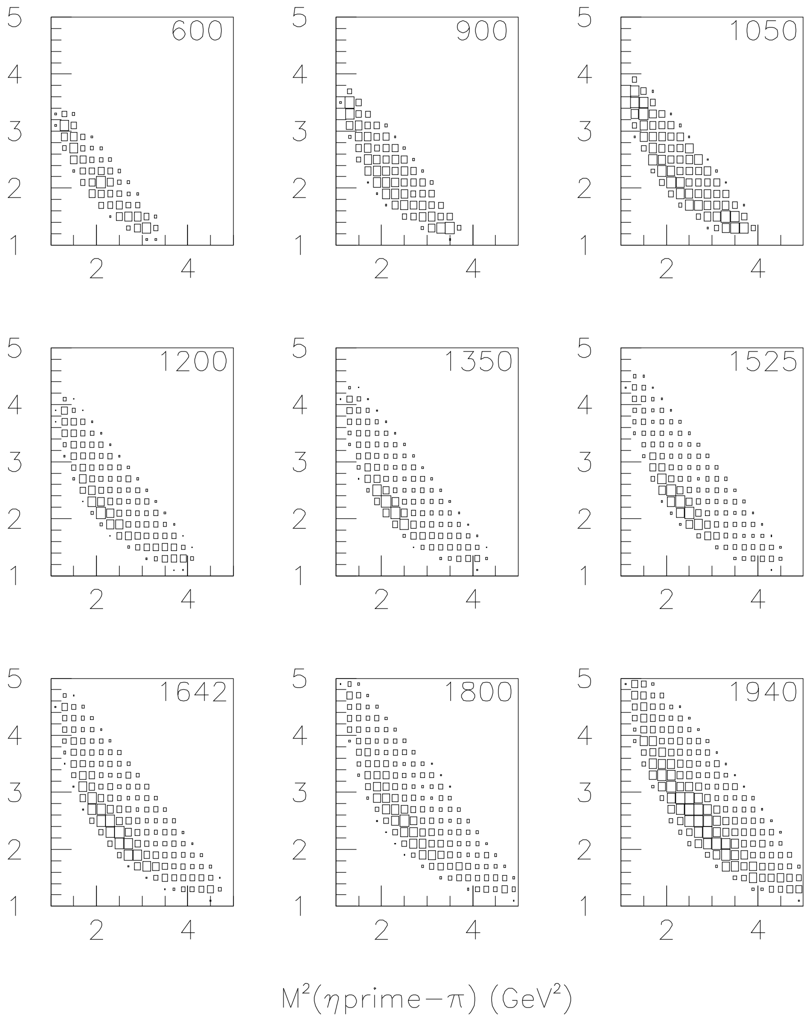

Fig. 2. Dalitz plots at all beam momenta for events from the signal region of Fig. 1. Numerical values indicate beam momenta in Mev/c.

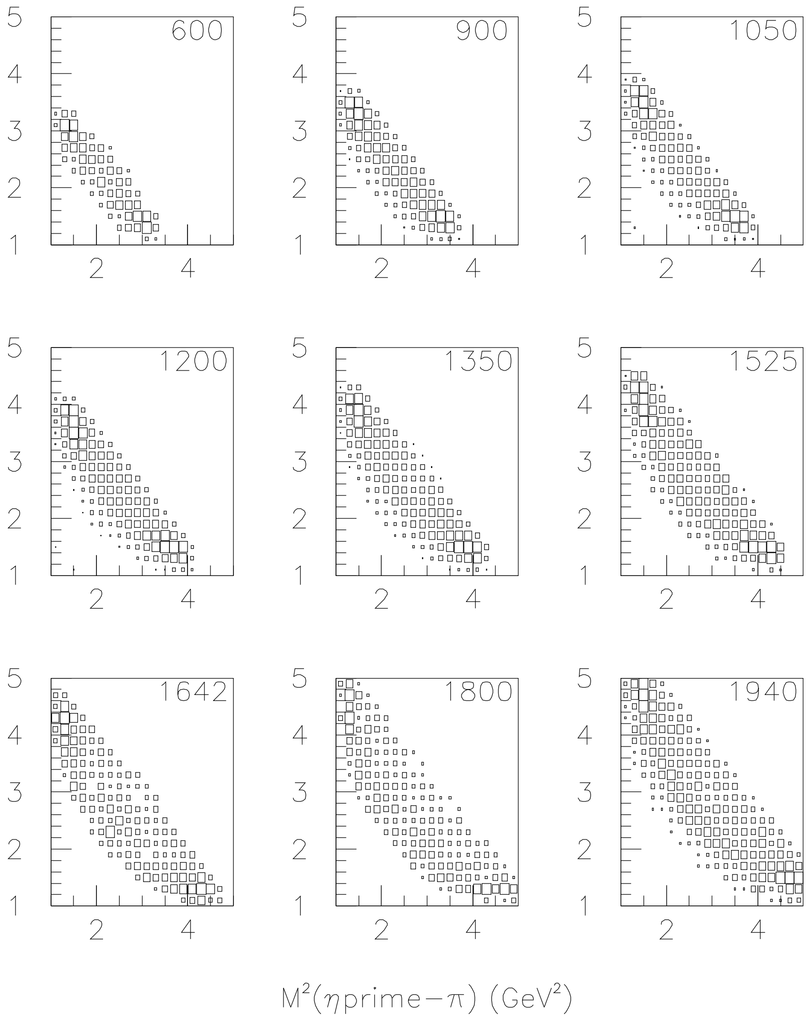

Fig. 3. Dalitz plots for events from the sidebin regions of Fig. 1.

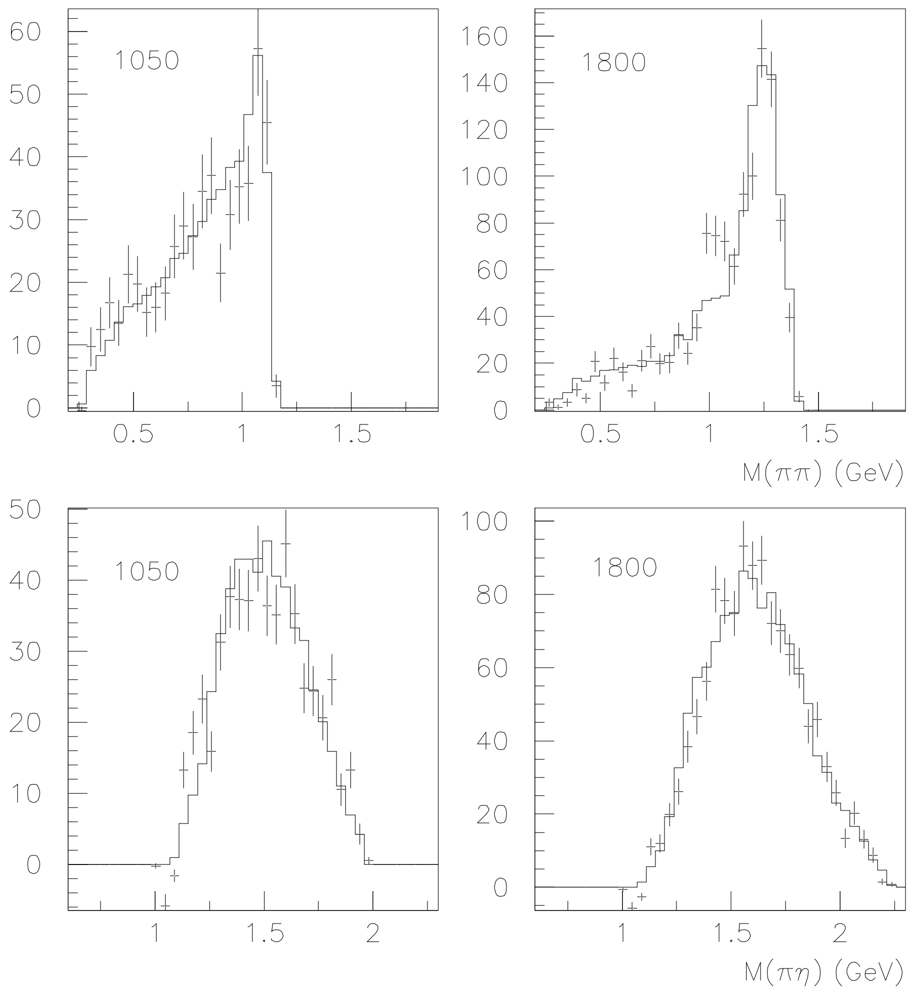

Fig. 4. Projections on to $M(\pi\pi)$ and $M(\eta'\pi)$ at beam momenta of 1050 and 1800 MeV/c; in all cases, a background subtraction is made using sidebins. Histograms show the fit compared with data.

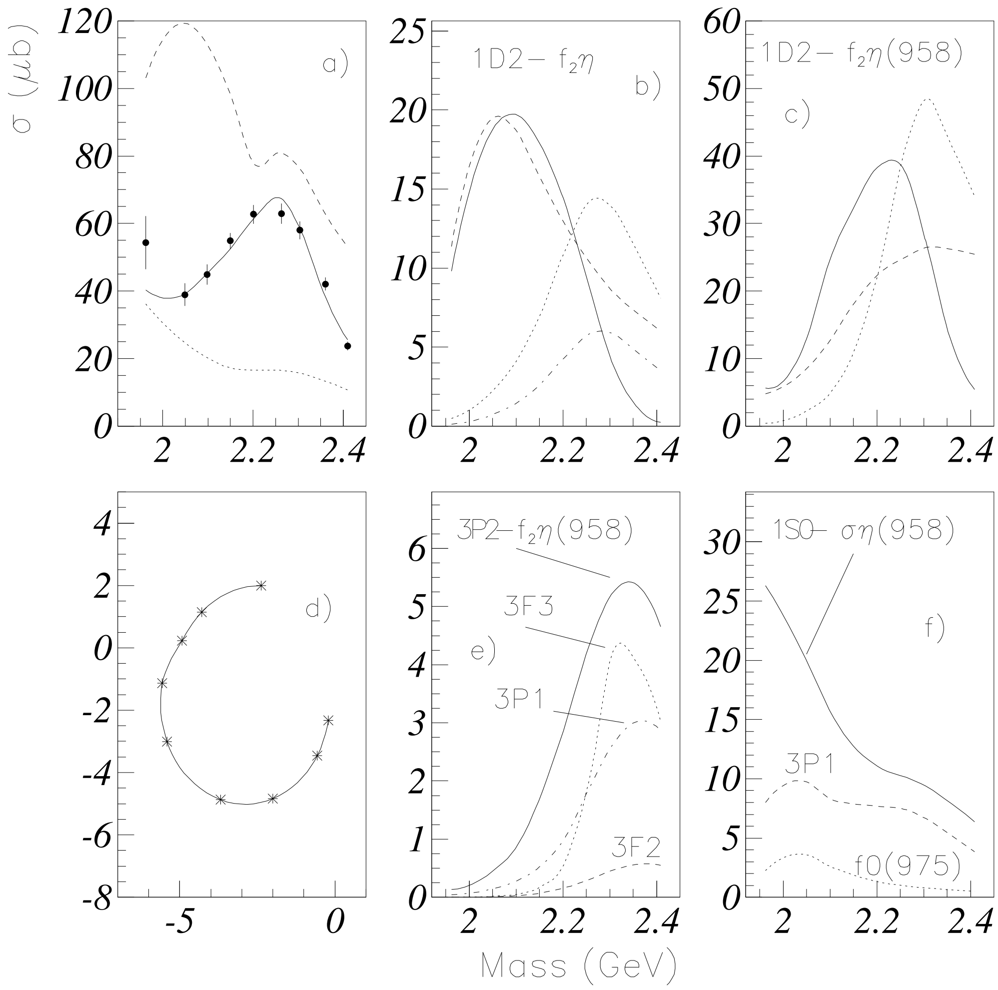

Fig. 5. (a) Points with errors show the integrated cross sections for the final state $\eta'\pi^0\pi^0$, after correction for backgrounds and for all decay modes of η', η and π^0; the full curve shows the fit from the amplitude analysis; the dashed curve shows the $\eta\pi\pi$ cross section from Ref. [3], multiplied by the SU(3) factor $(0.75)^2$; the dotted curve shows the $\sigma\eta'$ contribution; (b) the full curve shows the cross section for $f_2\eta$ fitted to $\eta\pi\pi$ data; the dotted curve shows the contribution from $\eta_2(2260)$ and the dashed curve that from $\eta_2(1860) + \eta_2(2030)$; the chain curve shows the intensity fitted to $f_2(1270)\eta$ with $L = 2$ in Ref. [4]; (c) as (b) for $f_2\eta'$; (d) Argand diagram for the $f_2\eta'$ S-wave amplitude; crosses mark beam momenta; (e) Intensities of contributions to $f_2\eta'$ from $^3P_2$ (full curve), $^3P_1$ (chain curve), $^3F_3$ (dotted) and $^3F_2$ (dashed); (f) Intensities of contributions to $\sigma\eta'$ from 0^- (full curve), 1^+ (dashed) and $1^+ \rightarrow f_0(975)\eta'$ (dotted).

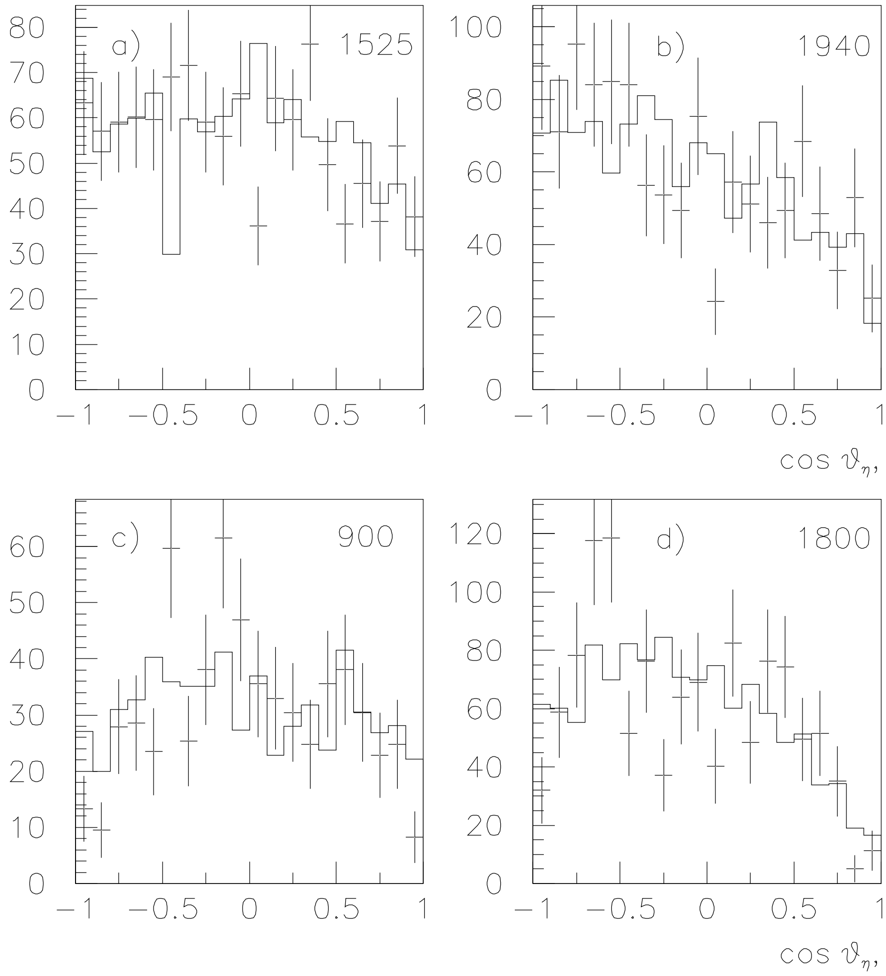

Fig. 6. Production angular distributions for $f_2\eta'$ at (a) 1525 and (b) 1940 MeV/c for $M(\pi\pi) > 1.1$ GeV; also for $\sigma\eta'$ at (c) 900 and (d) 1800 MeV/c for $M(\pi\pi) < 1$ GeV. Points with errors show data, uncorrected for acceptance; histograms show the maximum likelihood fit.